Influence of Polymer Structure and Architecture on Drug Loading and Redox-triggered Release

Peidong Wu[1], **Jingjing Gao**[1,2], **Priyaa Prasad**[1], **Kingshuk Dutta**[1], **Pintu Kanjilal**[1], **S. Thayumanavan**[1,3,4]

[1]Department of Chemistry, University of Massachusetts, Amherst, Massachusetts 01003, USA

[2]Current address: Center for Nanomedicine, Department of Anesthesiology, Perioperative and Pain Medicine, Brigham and Women's Hospital, Boston, MA 02115

[3]Department of Biomedical Engineering, University of Massachusetts Amherst, Amherst, Massachusetts, USA

[4]Center for Bioactive Delivery, The Institute for Applied Life Sciences, University of Massachusetts Amherst, Amherst, Massachusetts, USA

Abstract

Disulfide crosslinked nanoassemblies have attracted considerable attention as a drug delivery vehicle due to their responsiveness to the natural redox gradient in biology. Fundamentally understanding the factors that influence drug loading capacity, encapsulation stability, and precisely controlling the liberation of encapsulated cargo would be profoundly beneficial to redox responsive materials. Reported herein are block copolymer (BCP) based self-crosslinked nanogels, which exhibit high drug loading capacity, encapsulation stability, and controllable release kinetics. BCP nanogels show considerably higher loading capacity and better encapsulation stability under micromolar glutathione concentration than the random copolymer (RCP) nanogels. By partially substituting thiol-reactive pyridyl disulfide into the unreactive benzyl or butyl group, we observed opposite effects on the crosslinking process of BCP nanogels. We further studied the redox responsive cytotoxicity of our drug encapsulated nanogels in various cancer cell lines.
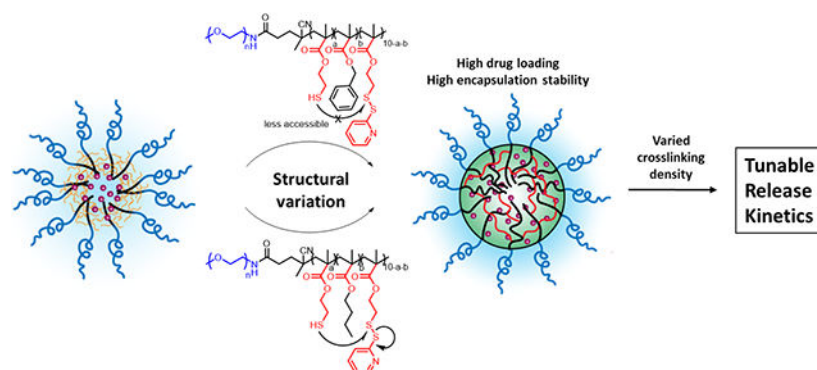
Graphical Abstract

Keywords

Drug Delivery; Polymer; Nanogel; Redox Responsive Release

INTRODUCTION

Redox responsive nanocarriers show enormous potential in intracellular drug delivery due to the natural redox gradient between intracellular and extracellular environments.[1-4] Typically, cytosolic glutathione (GSH) concentration reaches 10 mM, while extracellular GSH concentration lies between 2-20 µM.[5-7] Moreover, cytosolic GSH concentration in tumor cells is proven to be much higher than that in normal tissue,[8,9] which further stresses the importance of developing redox responsive drug delivery systems. Redox responsive scaffolds such as silica nanoparticles,[10] liposomes,[11] dendrimers,[12] and polymer-based drug delivery systems (nanoparticles, assemblies, gels)[13-19] have been explored for this purpose. Among them, amphiphilic polymeric drug delivery systems have been extensively studied due to the advantages of self-assemble nature and precise structural control.[20-22] One strategy to achieve redox-triggered release is to introduce redox-responsive linkage in between the hydrophilic compartment and the hydrophobic compartment of an amphiphilic block copolymer scaffold, which has been frequently used in micelle-type structures.[23,24] However, micellar nanocarriers normally suffer from premature drug release during circulation due to continuous interactions with proteins and cells within the bloodstream.[25,26] Post-formulation stabilization of drug encapsulated nanocarriers with redox-responsive crosslinkers provides an opportunity to not only prevent the undesirable drug release before reaching the target site but also enable triggerable release. Our group along with others has demonstrated the use of random copolymer (RCP) and block copolymer (BCP) based nanogels for this purpose, where crosslinking density could be varied to tune the cargo release kinetics.[27-31] In these systems, a thiol-reactive pyridine disulfide moiety act as the hydrophobic component while also allowing self-crosslinking of the amphiphilic assembly through disulfide exchange. When using pyridine disulfide, while the self-crosslinking process increases the steric barrier for encapsulated molecules to leak, it also causes a significant change in the hydrophilic-hydrophobic balance of the overall assembly as the aromatic pyridyl group is lost during the crosslinking event. This feature influences both the loading capacity and the encapsulation stability of the hydrophobic cargo.

To better understand the balance between the crosslinking-induced change in hydrophobic and hydrophilic balance and the encapsulation properties of the nanogels, we herein designed and studied a series of polymers. In this work, we compared block copolymer (BCP) based nanogels with the previously reported random copolymer (RCP) nanogels, to study the impact of the distribution of hydrophobic and hydrophilic units on drug encapsulation and release. To ensure that the encapsulated guest molecules are representative of the typical hydrophobicities encountered in small molecule drugs, we use chemotherapeutic drugs (camptothecin, paclitaxel, rapamycin, docetaxel) with varying hydrophobicity. To understand the crosslinking-induced gain in encapsulation stability along with the concurrent loss in hydrophobicity of the nanogel interior, we report a series of BCPs where different percentages of the reactive pyridyl disulfide (PDS) moieties are substituted with unreactive benzyl and butyl groups. With these substitutions, we are able to systematically tune the residual hydrophobicity of the crosslinked nanogels in the form of aromatic (benzyl) or aliphatic (butyl) residues. Finally, we report on the performance of the drug encapsulated nanogels in vitro to better understand the correlation between the release kinetics in aqueous media and drug-induced cytotoxicity.

EXPERIMENTAL

Materials.

All reagents were from commercial sources and used as received. All chemicals, 4-cyano-4-(phenylcarbonothioylthio)pentanoic acid, poly(ethyleneglycol)methylether(4-cyano-4-pentanoate dodecyl trithiocarbonate) (average Mw 1400, 5400, 10000), methacryloyl chloride, dichloromethane (DCM), triethylamine (TEA), 2,2'-dithiodipyridine, 2-mercaptoethanol, benzyl methacrylate, butyl methacrylate, tris(2-carboxyethyl)phosphine hydrochloride, glutathione (GSH), were obtained from Sigma-Aldrich; camptothecin, rapamycin, and paclitaxel were obtained from Selleckchem. All chemicals were used without further purification unless otherwise mentioned. 2,2′-Azobis-(2-methylpropionitrile) (AIBN) was procured from Sigma-Aldrich and purified by recrystallization before usage. Tetrahydrofuran (THF) was freshly distilled before each use. Other molecules without synthetic details shown were prepared using previously reported procedures.

Material synthesis.

Monomer pyridyl disulfide methacrylate (PDSMA) was synthesized according to previously reported procedures.[27] A solution of RAFT reagent, monomer(s), and AIBN in THF (200 μL) was degassed by three freeze-pump-thaw cycles before being sealed off under argon protection and vacuum. After 6 h at 65 °C, the polymerization media was diluted with 5 mL dichloromethane and condensed using rotavap, precipitated in diethyl ether for 3 times to remove unreacted monomers. The precipitate was collected and dried under a vacuum. The feed ratio for each polymer was listed in Table S1.

Polymer characterization.

NMR spectra were recorded on a Bruker DPX-400 MHz NMR spectrometer using the residual proton or carbon resonance of the solvent as the internal standard. The molecular

weight of the polymers was measured by gel permeation chromatography (GPC, Agilent) using a PMMA standard with a refractive index detector. THF was used as eluent with a flow rate of 1 mL/min.

Nanogels formulation and characterization.

Polymer (5 mg) and a calculated amount of drug were dissolved in 150 μL DMSO. The mixture was placed in a sonication bath followed by direct addition of 1 mL water, the solution was kept sonicating for 2 mins. The uniform micelle solution was then sonicated for 10 mins. The mixture was dialyzed against water for at least 6 h to remove the organic solvent. The amount of TCEP for nanoassembly crosslinking was listed in Table S2 to generate varied crosslinking density. After adding a calculated amount of TCEP, the solution was stirred for 6 h at room temperature and dialyzed against water for at least 6 h to remove the byproducts generated during crosslinking. Nanogel solution was then normalized back to 5 mg/mL and ready to use. The sizes of nanogels were characterized by DLS and TEM.

Drug encapsulation quantification.

Drug loading capacity and drug loading efficiency were calculated based on the equation below.

$$\text{Loading efficiency} = \frac{Weight\ of\ the\ encapsulated\ drug}{Weight\ of\ the\ drug\ initially\ added} \times 100\%$$

$$\text{Loading capacity} = \frac{Weight\ of\ the\ encapsulated\ drug}{weight\ of\ the\ polymer} \times 100\%$$

Camptothecin quantification was based on the UV absorbance at 365 nm in 90% (v/v) DMSO/water. The standard curve for CPT was shown in Figure S5a. UV-vis absorption spectra were obtained by a Cary 100 Scan spectrometer using quartz cuvettes. Rapamycin, docetaxel, and paclitaxel were quantified by HPLC. Durg encapsulated nanogels were first lyophilized then dissolved in MeCN with the addition of 10X excess of TCEP to decrosslink the nanogels for 6h. The solution was diluted to 0.1 mg/mL (polymer) and filtered with a 0.45 μm PTFE filter before further analysis with HPLC. The UV collector was set to 227 nm for rapamycin, docetaxel, and paclitaxel. The standard plots of drugs were shown in Figure S5b, c, d.

Nanogel stability and release kinetics study.

We first prepared 500 μL CPT (0.1 mg/mL) encapsulated nanogels. Then, 500 μL of 20 mM GSH solution (release kinetics) or 20 μM GSH solution (encapsulation stability) was added. The stability and release kinetics study was carried out by monitoring the change of CPT UV absorbance at 370 nm. UV-vis absorption spectra were obtained by a Cary 100 Scan spectrometer using disposable sizing cuvettes.

Cell culture.

Human breast cancer cell lines MDA-MB-231 and MCF-7, a fibrosarcoma cell line HT-1080, a human osteosarcoma cell line SAOS-2, a human prostate cancer cell line were grown in T75 cell culture flask containing Dulbecco's Modified Eagle Medium

supplemented with 10% (FBS), 1% l-glutamine, and 1% antibiotic-antimycotic (comprised of 100 units/mL penicillin and 100 μg/mL of streptomycin). All cells were grown at 5% CO_2 and 37 °C.

Cell viability with MTT assay.

All five cells were seeded on flat-bottom 96-well tissue culture plates at a density of 5000 cells/well and rested for 24 h at 37 °C in 5% CO_2. After incubation, the culture medium was removed, and cells were treated with nanogel samples at different concentrations (0.05 mg/mL to 1 mg/mL) in complete medium for 48 h. After treatments, cells were washed, and the medium was replaced with 3-(4,5-dimethylthiazol-2-yl) 2,5-diphenyltetrazolium solution (MTT) (prepared as 0.5 mg/mL in medium) and further incubated for 3–4 h at 37 °C. Remove 75 μL of medium and add 50 μL DMSO to each well and incubate at 37 °C for another 10 mins. The purple color formation was observed and recorded using a plate reader at 540 nm.

RESULT AND DISCUSSION

Synthesis and characterization of BCP and RCP.

To compare BCP- and RCP-based nanogels, we first synthesized a series of BCPs (BCP_{1000}, BCP_{5000}, BCP_{10000}), and an RCP using reversible addition-fragmentation chain transfer (RAFT) polymerization and characterized them using ^{1}H NMR and GPC. In the BCPs, the hydrophobic block is maintained at 10 repeat units of PDS-methacrylate while tuning the PEG chain length in the hydrophilic block is varied with an Mn 1000, 5000, or 10000. Synthesis of these polymers was conveniently achieved using commercially available PEG-RAFT as the initiator (Figure 1). An RCP was also synthesized with 30% PEG-methacrylate and 70% PDS-methacrylate as the co-monomers, as this ratio was optimized in our previous studies[27,32]. For all polymers, the ratio between PEG moiety and PDS moiety was confirmed by ^{1}H NMR (Table 1).

Polymeric micelle formulation and crosslinking study.

With the polymers in hand, we first investigated the self-assembly behavior of BCPs in the aqueous phase and the crosslinking process to generate the BCP-based nanogels (Figure 2a, b). Polymers were directly dissolved in water and sonicated until the solution becomes transparent. Size distribution of polymeric micelles was found to be ~220 nm, 60 nm, and 350 nm from BCP_{1000}, BCP_{5000}, and BCP_{10000} respectively, as characterized by dynamic light scattering (DLS) (Figure 2c, Figure S2a). Transmission electron microscopy (TEM) analysis of the BCP_{5000} assembly is found to be consistent with the DLS data (Figure 2c). For RCP, we observed 10 nm assemblies which are consistent with our previous results[27]. As nanocarriers with diameters <200nm are generally considered desirable for drug delivery systems,[33-35] BCP_{5000} was chosen for further study. The micellar type of assembly was further crosslinked by adding a calculated number of tris(2-carboxyethyl)phosphine (TCEP) based on the amount of PDS. The crosslink density was calculated by monitoring the UV absorbance of the pyridothione byproduct at 343 nm[27]. From 0.2 eq to 5 eq of TCEP was used for crosslinking the BCP_{5000} micelles. We observed a steady increase in the formation of pyridothione with increasing TCEP equivalence. When more than 2 eq of TCEP was

applied, the formation of pyridothione reached a plateau, and yet the maximum crosslinking density could reach only ~60% for the BCP_{5000} nanogel. This is likely due to the possibility that the densely crosslinked hydrophobic core in the BCP assembly prevents TCEP from accessing and further crosslinking.

Preparation and characterization of drug encapsulated nanogel.

After studying the self-assembly behavior of BCPs and crosslinking process, we optimized the method of drug encapsulation. Taking the concept of the recent formulation techniques such as flash nanoprecipitation and microfluidic devices methods[36,37], we modified our previous preparation method where instead of slowly stirring while adding antisolvent dropwise, we directly added 1 mL water to the polymer and drug mixture in DMSO (~ 60 μL) with immediate sonication. Stable and reproducible micelle solutions can be prepared within 10 mins. The drug encapsulated micelle solution was dialyzed against water to remove the organic solvents. Then, both RCP and BCP_{5000} micelles were crosslinked with 12.5, 25, or 50 mol% (against the amount of PDS groups within the polymers) of TCEP targeting for 25%, 50%, and 100% crosslinking, assuming 100% crosslinking efficiency. Our estimations, based on pyridothione release, indicate that the actual cross-linking densities correspond to 23%, 46%, and 70% for RCPs, and 13%, 24%, and 39% for BCP_{5000}s. Sizes of the drug-encapsulated nanogels were characterized by DLS, where drug encapsulated BCP_{5000} nanogels and RCP nanogels were found to be ~200 nm and 300 nm, respectively (Figure S3a, b). Also, the degree of crosslinking did not affect the size of the assemblies. The similarity in sizes offers a better opportunity to directly compare these nanogels for their encapsulation properties, outlined below.

Drug loading capacity and efficiency.

To evaluate the drug loading capacity and efficiency of the BCP_{5000} and RCP nanogel, CPT is used as the model drug because it offers to be conveniently assessed using its UV absorbance at 365 nm (Figure S5). We first evaluated the loading efficiency of BCP_{5000} nanogel with different feed ratios ranging from 2% to 40%. As a significant drop in loading efficiency was observed at 40% feed, we chose 30% feed ratio for further experiments (Figure S6a). The loading efficiency of BCP_{5000} drug loading efficiency (DLE) and drug loading capacity (DLC) for RCP and BCP_{5000} are summarized in Figure 3a, where BCP_{5000} exhibits a consistently high DLE of >90%. On the other hand, RCP shows a significantly lower DLC with a maximum of 20% at 25% crosslinking. The extent of crosslinking shows a considerable impact on the loading capacity of nanogels from RCP, which is attributed to the continuous loss of hydrophobicity of the assemblies during the crosslinking process. For nanogels from BCPs, interestingly, crosslinking has little to no effect on the DLC.

Encapsulation stability and redox responsive release kinetics.

Apart from the loading capacity, we also investigated the encapsulation stability of BCP and RCP nanogels under μM and mM glutathione (GSH) concentrations. Camptothecin-encapsulated nanogels with various crosslinking densities were placed under low GSH concentration (10 μM), mimicking the extracellular environment during the circulation. Nanogels from BCP_{5000} show superior stability, compared to RCP nanogel, under 10 μM GSH for five days, where the loss of drug is negligible. In contrast, about 10-15% drug

leakage was observed after five days for the RCP nanogels with different crosslinking density (Figure 3b). Next, we exposed these drug-encapsulated nanogels to 10 mM GSH (corresponds to intracellular GSH concentration) to evaluate their redox responsiveness. From their release profile, RCP shows a faster and more complete release. Note that, for the same weight of BCP_{5000} and RCP, the amount of disulfide bonds in RCP is higher than that in BCP_{5000}. However, the release kinetics for RCP is faster than BCP_{5000}, which indicates that the release kinetics of nanogel is not only determined by the amount of disulfide crosslinking alone but is presumably sensitive to the polymer packing in the nanogels, which is determined by the polymer architecture. Also, the release profile could be fine-tuned by varying the crosslinking density for both RCP and BCP_{5000} nanogels, where a higher crosslinking degree results in more stable encapsulation and slower release kinetics (Figure 3c, 3d).

Design and synthesis of benzyl and butyl substituted BCP polymers.

To further understand the crosslinking-induced gain in encapsulation stability with concurrent loss in hydrophobicity of the nanogel interior, we designed and synthesized a series of BCPs where PDS units in the hydrophobic part were partially substituted by benzyl or butyl groups. Polymers were prepared using RAFT polymerization with a PEG_{5000} modified RAFT reagent and using pyridyl disulfide methacrylate (PDSMA), benzyl methacrylate (BnMA) or butyl methacrylate (BuMA) as monomers. Structural variations of benzyl substituted block copolymers (PBns) and butyl substituted block copolymers (PBus) are listed in Table 2. Sizes from all these polymers assemblies were characterized by DLS, which were found to be ~50 nm and remain unchanged at the different extent of crosslinking (Figure S2).

Structural effect on loading stability and release kinetics.

Next, we evaluated the structural effect on encapsulation stability and release kinetics. Camptothecin-encapsulated nanogels were prepared as described above, where PBn and PBu nanogels were crosslinked by 12.5, 25, and 50 mol% of TCEP, the actual crosslinking density of these nanogels were listed in the brackets. Then, these nanogels were placed in 10 μM GSH solution to study their encapsulation stability. Negligible release of CPT was observed from nanogels made from PBns or PBus (Figure 4a, 4b), which indicates that the substitution of PDS with benzyl or butyl units does not influence encapsulation stability. Then we treated these drug-encapsulated nanogels with 10 mM GSH to investigate their release kinetics. First, we are interested in understanding the substitution effect from reactive PDS moieties to unreactive benzyl moieties on release kinetics. In contrast to BCP_{5000}, the release rate of CPT in PBn nanogels is slower at low crosslinking density than that at high crosslinking density (Figure 5a, 5b, 5c). This can be explained by the nature of the crosslinking process, which is a stepwise reaction that a free thiol is generated first, followed by a thiol-disulfide exchange with a nearby PDS group to form a disulfide bond crosslinker. The availability for the second step is determined by the accessibility of the nearby PDS. Therefore, we hypothesize that benzyl moiety within the hydrophobic core inhibits the crosslinking process, where the TCEP-generated free thiol less readily forms the disulfide crosslinker due to the limited accessibility to other PDS moieties. This might be because of the rigid nature of the benzyl-polymer core, presumably due to the stronger

interaction between benzyl moiety, PDS moiety, and CPT drug through both hydrophobic and π-π interaction (Figure 6). However, PBu_{10} and PBu_{60} nanogels showed a similar trend as BCP_{5000}, where at a high extent crosslinking the release rate of CPT decreased (Figure 5d, 5e). This also indicates that butyl groups do not inhibit the crosslinking process as significantly as the benzyl groups. Similarly, a higher extent of crosslinking leads to a slightly higher release rate even for PBu_{80}, which also might be due to the limited amount of PDS that could be utilized during the crosslinking process (Figure 5f).

Drug loading property of structural variant polymers.

To evaluate the impact of the structural variations in the guest molecule on its loading inside the nanogel, drugs with varied *log P* values were encapsulated into the BCP nanogels and the drug loading capacity was characterized. In this section, we picked PBn_{60} and PBu_{60} from the two types of substitutions. We characterized the morphology of drug-encapsulated nanogels with both DLS and TEM, where these drug-encapsulated nanogels show a consistent size of around 200 nm (figure S3, S4). We further evaluated the impact of partially substituting PDS into benzyl or butyl on drug loading. Neglectable differences on DLC and DLE were observed between these structural variations, indicating the structural change by partial substitution does not influence the hydrophobic interaction between the polymers and drugs (Figure S6b,c). Similarly, crosslinking density also does not affect DLE and DLC, as previously observed in BCP_{5000}. To further evaluate the applicability of our nanocarrier for other drugs with different l*og P* values, DLC and DLE of rapamycin and paclitaxel were also characterized (Table 3). As the UV absorbances of rapamycin and paclitaxel overlap with the polymer, the encapsulated drugs were characterized by HPLC. With 30 wt% initial loadings, all three drugs can be efficiently encapsulated, suggesting that these nanogels can accommodate drug molecules with a range of *log P* values.

Redox-responsive cytotoxicity.

Since our BCP nanogels are capable of encapsulating a variety of drug molecules with tunable release kinetics, we study their performance in vitro. First, we investigated the efficiency of the drug-loaded nanogels in a human prostate cancer cell line, DU-145. BCP_{5000} nanogel was utilized to encapsulate paclitaxel, rapamycin, and docetaxel and compared their cytotoxicity with free drugs. The free nanocarrier is non-toxic to the cells, and the free drugs showed better toxicity than the drug encapsulated nanogels (Figure 7a). Next, we were interested in studying the effect of crosslinking density on drug release kinetics in vitro. We hypothesized that slower release kinetics would cause less cell death. BCP_{5000} nanogels with varied crosslinking density from 13% to 39% were prepared and dosed to DU-145 cells at 0.5, 1, and 10 μM (based on drug concentration) for 48 h. We observed that higher crosslinking density did indeed cause lesser cytotoxicity (Figure 7b). However, the differences in cytotoxicity are not significant, which could be due to the high sensitivity of the DU-145 cell line to paclitaxel. At 0.5, 1, and 10 μM of free paclitaxel, the cytotoxicity to DU-145 cells was similar (supporting information Figure S7a), which suggests that 0.5 μM drug dosage is already at saturation concentration. Therefore, it is reasonable that the release kinetics would not influence cytotoxicity significantly. To further test our hypothesis, the relationship between payload release kinetics and cell apoptosis rate was studied in four other cancer cell lines. To find an appropriate drug dosage, we

first screened the cytotoxicity of camptothecin in all four cell lines (Figure S8). Based on the results, we selected 0.25 μg/mL for MDA-MB-231 and MCF-7 cell lines, and 0.05 μg/mL for SAOS-2 and HT-1080 cell lines. Meanwhile, we also decreased the amount of encapsulated drug in each nanogels from 30 wt% to 20 wt%. Control nanogels without CPT loading did not show toxicity to cells even at 0.1 mg/mL (Supporting information Figure S7b, c). A clear trend following our previous release profile upon 10 mM GSH was observed, where slower release kinetics is well-correlated with lesser cytotoxicity in MDA-MB-231 and MCF-7 cell lines (Figure 7c, 7d). Significant differences in cytotoxicity were observed by varied crosslinking density within each type of nanogels, where for nanogels from PBn_{10}, PBn_{60}, and PBn_{80} higher crosslinking density causes higher toxicity; for nanogels from PBu_{60} and BCP_{5000} higher crosslinking density causes lower toxicity. Also, higher benzyl substitution from PBn_{10} to PBn_{80} caused an increase in cytotoxicity, which is attributed to the faster release of payload. The release kinetics of nanogels upon 10 mM GSH in the test tube shows a significant difference only at 120 h time period. However, the in vitro environment is far more complex than solely GSH; therefore, it is possible that the release of the payload is accelerated in cells. But, it is noteworthy that the relative trends remain the same in both the test tube and in vitro. In both MDA-MB-231 and MCF-7 cell lines, toxicity differences in 24 h are more significant than 48 h, which also indicate that the toxicity differences are due to the release kinetics. When the encapsulated drugs are completely released, all the nanogels should exhibit similar toxicity. In SAOS-2 and HT-1080 cell lines, we also observed a similar trend but not as significant as that in MDA-MB-231 and MCF-7 cell lines (supporting information S9), which is likely due to the sensitivity differences among cell lines to the cytotoxic cargo.

CONCLUSIONS

In summary, RCP and BCP nanogels were successfully prepared in aqueous media and were evaluated for their drug loading, encapsulation stability, and release kinetics. The BCP nanogel shows higher drug loading capacity (~30 wt%) and enhanced encapsulation stability. To further understand the crosslinking-induced gain in encapsulation stability with concurrent loss in hydrophobicity of the nanogel interior, we designed and synthesized a series of BCPs where PDS units in the hydrophobic part are partially substituted with benzyl or butyl groups. Such substitution variations or crosslinking density differences did not significantly impact the drug loading or the encapsulation stability of BCP nanogels. The extent of crosslinking density does however impact the redox-triggered drug release kinetics. Interestingly, introducing benzyl and butyl groups into the hydrophobic block of the BCP nanogels provides opposite effects, where PBns show accelerated release kinetics at higher crosslinking while PBus follow the anticipated trend where higher crosslinking density leads to a slow release rate. This difference is attributed to the variations in the packing of the polymer chains, which affect the accessibility of the PDS units during the crosslinking process. Moreover, BCP nanogels are capable of encapsulating a variety of drug molecules at high drug loading capacity. In vitro study in various cancer cell lines support our hypothesis that cytotoxicity of drug encapsulated nanogels correlates with their redox-triggered payload release kinetics. Together, these data suggest that the nanogels described here hold enormous potential as drug delivery systems, as precise control of

payload release provides new avenues towards the design of next-generation nanocarriers and redox responsive materials.

Supplementary Material

Refer to Web version on PubMed Central for supplementary material.

ACKNOWLEDGMENT

REFERENCES

(1). McCarley RL Redox-Responsive Delivery Systems. Annu. Rev. Anal. Chem 2012, 5, 391–411. 10.1146/annurev-anchem-062011-143157.

(2). Guo X; Cheng Y; Zhao X; Luo Y; Chen J; Yuan W-E Advances in Redox-Responsive Drug Delivery Systems of Tumor Microenvironment. J. Nanobiotechnology 2018 161 2018, 16 (1), 1–10. 10.1186/S12951-018-0398-2. [PubMed: 29321058]

(3). Dutta K; Das R; Medeiros J; Thayumanavan S Disulfide Bridging Strategies in Viral and Nonviral Platforms for Nucleic Acid Delivery. Biochemistry 2021, 60 (13), 966–990. 10.1021/acs.biochem.0c00860. [PubMed: 33428850]

(4). Chacko RT; Ventura J; Zhuang J; Thayumanavan S Polymer Nanogels: A Versatile Nanoscopic Drug Delivery Platform. Adv. Drug Deliv. Rev 2012, 64 (9), 836–851. 10.1016/j.addr.2012.02.002. [PubMed: 22342438]

(5). Hwang C; Sinskey AJ; Lodish HF Oxidized Redox State of Glutathione in the Endoplasmic Reticulum. Science (80-.). 1992, 257 (5076), 1496–1502. 10.1126/science.1523409.

(6). Mura S; Nicolas J; Couvreur P Stimuli-Responsive Nanocarriers for Drug Delivery. Nat. Mater 2013 1211 2013, 12 (11), 991–1003. 10.1038/nmat3776. [PubMed: 24150417]

(7). Lee MH; Yang Z; Lim CW; Lee YH; Dongbang S; Kang C; Kim JS Disulfide-Cleavage-Triggered Chemosensors and Their Biological Applications. Chem. Rev 2013, 113 (7), 5071–5109. 10.1021/CR300358B. [PubMed: 23577659]

(8). McLellan LI; Wolf CR Glutathione and Glutathione-Dependent Enzymes in Cancer Drug Resistance. Drug Resist. Updat 1999, 2 (3), 153–164. 10.1054/DRUP.1999.0083. [PubMed: 11504486]

(9). Tew KD Glutathione-Associated Enzymes in Anticancer Drug Resistance. Cancer Res. 2016, 76 (1), 7–9. 10.1158/0008-5472.CAN-15-3143. [PubMed: 26729789]

(10). Maiti C; Parida S; Kayal S; Maiti S; Mandal M; Dhara D Redox-Responsive Core-Cross-Linked Block Copolymer Micelles for Overcoming Multidrug Resistance in Cancer Cells. ACS Appl. Mater. Interfaces 2018, 10 (6), 5318–5330. 10.1021/acsami.7b18245. [PubMed: 29355017]

(11). Chi Y; Yin X; Sun K; Feng S; Liu J; Chen D; Guo C; Wu Z Redox-Sensitive and Hyaluronic Acid Functionalized Liposomes for Cytoplasmic Drug Delivery to Osteosarcoma in Animal Models. J. Control. Release 2017, 261, 113–125. 10.1016/J.JCONREL.2017.06.027. [PubMed: 28666726]

(12). Laskar Partha; Somani Sukrut; Campbell S. Jane; Mullin Margaret; Keating Patricia; Tate RJ; Irving Craig; Leung HY; Dufès Christine. Camptothecin-Based Dendrimersomes for Gene Delivery and Redox-Responsive Drug Delivery to Cancer Cells. Nanoscale 2019, 11 (42), 20058–20071. 10.1039/C9NR07254C. [PubMed: 31612185]

(13). Liu B; Wu R; Gong S; Xiao H; Thayumanavan S In Situ Formation of Polymeric Nanoassemblies Using an Efficient Reversible Click Reaction. Angew. Chemie - Int. Ed 2020, 59 (35), 15135–15140. 10.1002/anie.202004017.

(14). Gordon MR; Zhuang J; Ventura J; Li L; Raghupathi K; Thayumanavan S Biodistribution Analysis of NIR-Labeled Nanogels Using in Vivo FMT Imaging in Triple Negative

Human Mammary Carcinoma Models. Mol. Pharm 2018, 15 (3), 1180–1191. 10.1021/ ACS.MOLPHARMACEUT.7B01011. [PubMed: 29378144]

(15). Nakahata M; Takashima Y; Yamaguchi H; Harada A Redox-Responsive Self-Healing Materials Formed from Host–guest Polymers. Nat. Commun 2011, 2 (1), 1–6. 10.1038/ncomms1521.

(16). Deng Z; Yuan S; Xu RX; Liang H; Liu S Reduction-Triggered Transformation of Disulfide-Containing Micelles at Chemically Tunable Rates. Angew. Chemie Int. Ed 2018, 57 (29), 8896–8900. 10.1002/ANIE.201802909.

(17). Deng Z; Liu S Controlled Drug Delivery with Nanoassemblies of Redox-Responsive Prodrug and Polyprodrug Amphiphiles. J. Control. Release 2020, 326, 276–296. 10.1016/ J.JCONREL.2020.07.010. [PubMed: 32682899]

(18). Ang CY; Tan SY; Teh C; Lee JM; Wong MFE; Qu Q; Poh LQ; Li M; Zhang Y; Korzh V; Zhao Y Redox and PH Dual Responsive Polymer Based Nanoparticles for In Vivo Drug Delivery. Small 2017, 13 (7), 1602379. 10.1002/smll.201602379.

(19). Gao J; Liu X; Secinti H; Jiang Z; Munkhbat O; Xu Y; Guo X; Thayumanavan S Photoactivation of Ligands for Extrinsically and Intrinsically Triggered Disassembly of Amphiphilic Nanoassemblies. Chem. - A Eur. J 2018, 24 (8), 1789–1794. 10.1002/chem.201705217.

(20). Ryu J-H; Bickerton S; Zhuang J; Thayumanavan S Ligand-Decorated Nanogels: Fast One-Pot Synthesis and Cellular Targeting. Biomacromolecules 2012, 13 (5), 1515–1522. 10.1021/ BM300201X. [PubMed: 22455467]

(21). Li L; Raghupathi K; Yuan C; Thayumanavan S Surface Charge Generation in Nanogels for Activated Cellular Uptake at Tumor-Relevant PH. Chem. Sci 2013, 4 (9), 3654–3660. 10.1039/ C3SC50899D.

(22). Zhuang J; Chacko R; Torres DFA; Wang H; Thayumanavan S Dual Stimuli–Dual Response Nanoassemblies Prepared from a Simple Homopolymer. ACS Macro Lett. 2013, 3 (1), 1–5. 10.1021/MZ400515S.

(23). Klaikherd A; Nagamani C; Thayumanavan S Multi-Stimuli Sensitive Amphiphilic Block Copolymer Assemblies. J. Am. Chem. Soc 2009, 131 (13), 4830–4838. 10.1021/JA809475A. [PubMed: 19290632]

(24). Ma N; Li Y; Xu H; Wang Z; Zhang X Dual Redox Responsive Assemblies Formed from Diselenide Block Copolymers. J. Am. Chem. Soc 2009, 132 (2), 442–443. 10.1021/JA908124G.

(25). Gong J; Chen M; Zheng Y; Wang S; Wang Y Polymeric Micelles Drug Delivery System in Oncology. J. Control. Release 2012, 159 (3), 312–323. 10.1016/J.JCONREL.2011.12.012. [PubMed: 22285551]

(26). Lu Y; Zhang E; Yang J; Cao Z Strategies to Improve Micelle Stability for Drug Delivery. Nano Res. 2018 1110 2018, 11 (10), 4985–4998. 10.1007/S12274-018-2152-3. [PubMed: 30370014]

(27). Ryu JH; Chacko RT; Jiwpanich S; Bickerton S; Babu RP; Thayumanavan S Self-Cross-Linked Polymer Nanogels: A Versatile Nanoscopic Drug Delivery Platform. J. Am. Chem. Soc 2010, 132 (48), 17227–17235. 10.1021/ja1069932. [PubMed: 21077674]

(28). Gao J; Wu P; Fernandez A; Zhuang J; Thayumanavan S Cellular AND Gates: Synergistic Recognition to Boost Selective Uptake of Polymeric Nanoassemblies. Angew. Chemie - Int. Ed 2020, 59 (26), 10456–10460. 10.1002/anie.202002748.

(29). Gao J; Dutta K; Zhuang J; Thayumanavan S Cellular- and Subcellular-Targeted Delivery Using a Simple All-in-One Polymeric Nanoassembly. Angew. Chemie 2020, 132 (52), 23672–23676. 10.1002/ange.202008272.

(30). R. B. KC; Xu P Multicompartment Intracellular Self-Expanding Nanogel for Targeted Delivery of Drug Cocktail. Adv. Mater 2012, 24 (48), 6479–6483. 10.1002/ADMA.201202687. [PubMed: 23001909]

(31). Chen W; Zou Y; Jia J; Meng F; Cheng R; Deng C; Feijen J; Zhong Z Functional Poly(ε-Caprolactone)s via Copolymerization of ε-Caprolactone and Pyridyl Disulfide-Containing Cyclic Carbonate: Controlled Synthesis and Facile Access to Reduction-Sensitive Biodegradable Graft Copolymer Micelles. Macromolecules 2013, 46 (3), 699–707. 10.1021/MA302499A.

(32). Ryu JH; Jiwpanich S; Chacko R; Bickerton S; Thayumanavan S Surface-Functionalizable Polymer Nanogels with Facile Hydrophobic Guest Encapsulation Capabilities. J. Am. Chem. Soc 2010, 132 (24), 8246–8247. 10.1021/ja102316a. [PubMed: 20504022]

(33). Maeda H; Matsumura Y Tumoritropic and Lymphotropic Principles of Macromolecular Drugs. Crit. Rev. Ther. Drug Carrier Syst 1989, 6 (3), 193–210. [PubMed: 2692843]

(34). Maeda H; Fang J; Inutsuka T; Kitamoto Y Vascular Permeability Enhancement in Solid Tumor: Various Factors, Mechanisms Involved and Its Implications. In International Immunopharmacology; Elsevier, 2003; Vol. 3, pp 319–328. 10.1016/S1567-5769(02)00271-0. [PubMed: 12639809]

(35). Maeda H The Enhanced Permeability and Retention (EPR) Effect in Tumor Vasculature: The Key Role of Tumor-Selective Macromolecular Drug Targeting. Adv. Enzyme Regul 2001, 41 (1), 189–207. 10.1016/S0065-2571(00)00013-3. [PubMed: 11384745]

(36). Markwalter CE; Pagels RF; Wilson BK; Ristroph KD; Prud'homme RK Flash Nanoprecipitation for the Encapsulation of Hydrophobic and Hydrophilic Compounds in Polymeric Nanoparticles. J. Vis. Exp 2019, 2019 (143), e58757. 10.3791/58757.

(37). Ran R; Sun Q; Baby T; Wibowo D; Middelberg APJ; Zhao CX Multiphase Microfluidic Synthesis of Micro- and Nanostructures for Pharmaceutical Applications. Chem. Eng. Sci 2017, 169, 78–96. 10.1016/j.ces.2017.01.008.
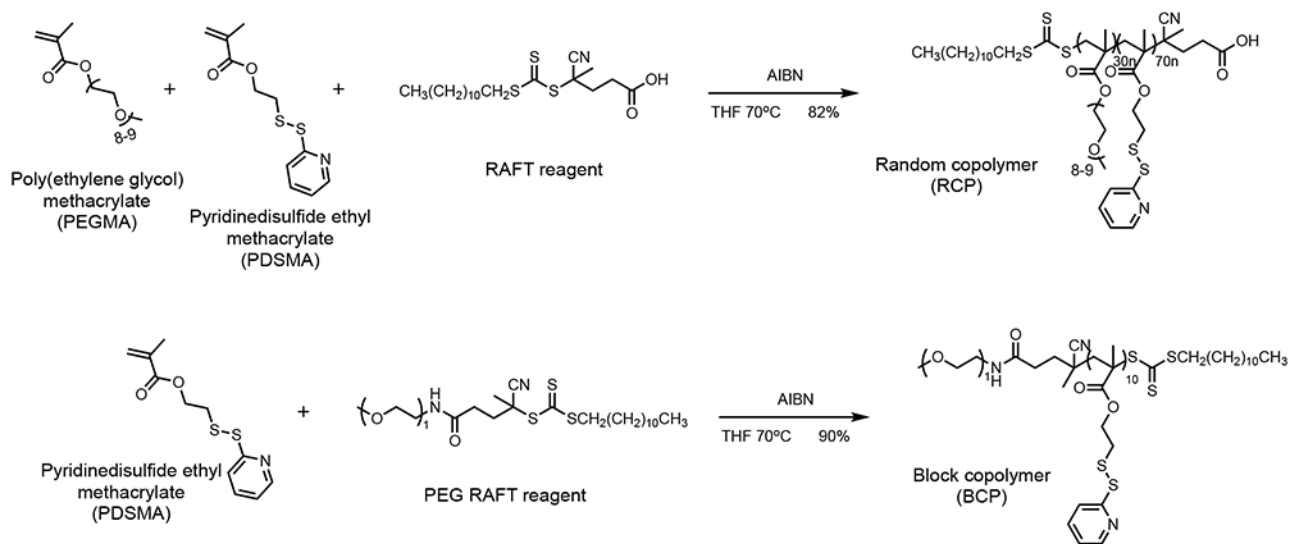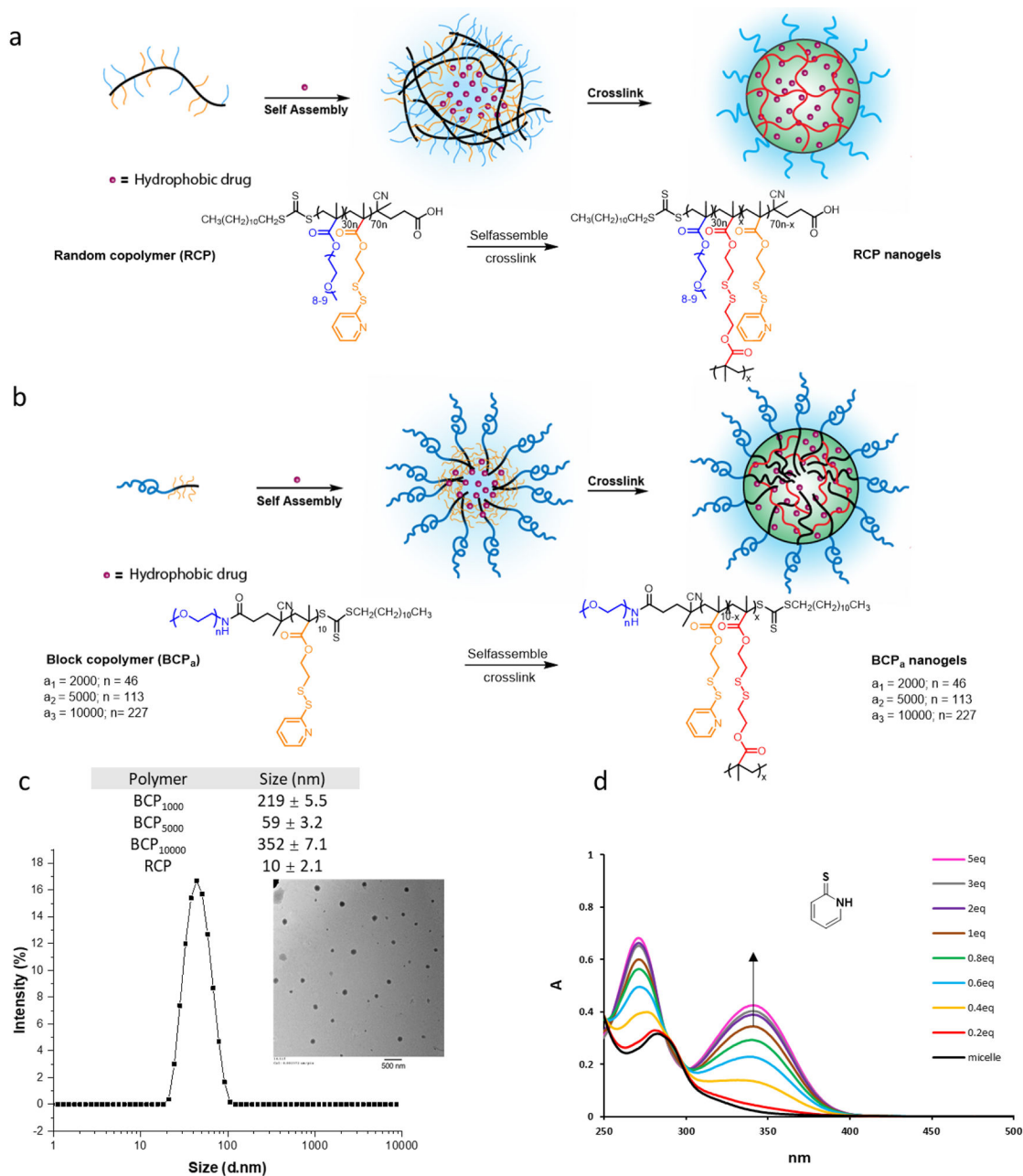
Figure 1.
Synthesis of the random copolymer and the block copolymers used in this study.

Figure 2.
(a) RCP self-assembly and crosslinking scheme; (b) BCP self-assembly and crosslinking scheme; (c) The size distribution of BPC micelles (0.2 mg/mL) by DLS (TEM image inside scale bar 500 nm); (d) TCEP dose-dependent crosslinking density variation for by monitoring the production of pyridothione at 343nm. Data was labeled by the ratio between TCEP and PDS (calculated from ^{1}H NMR).
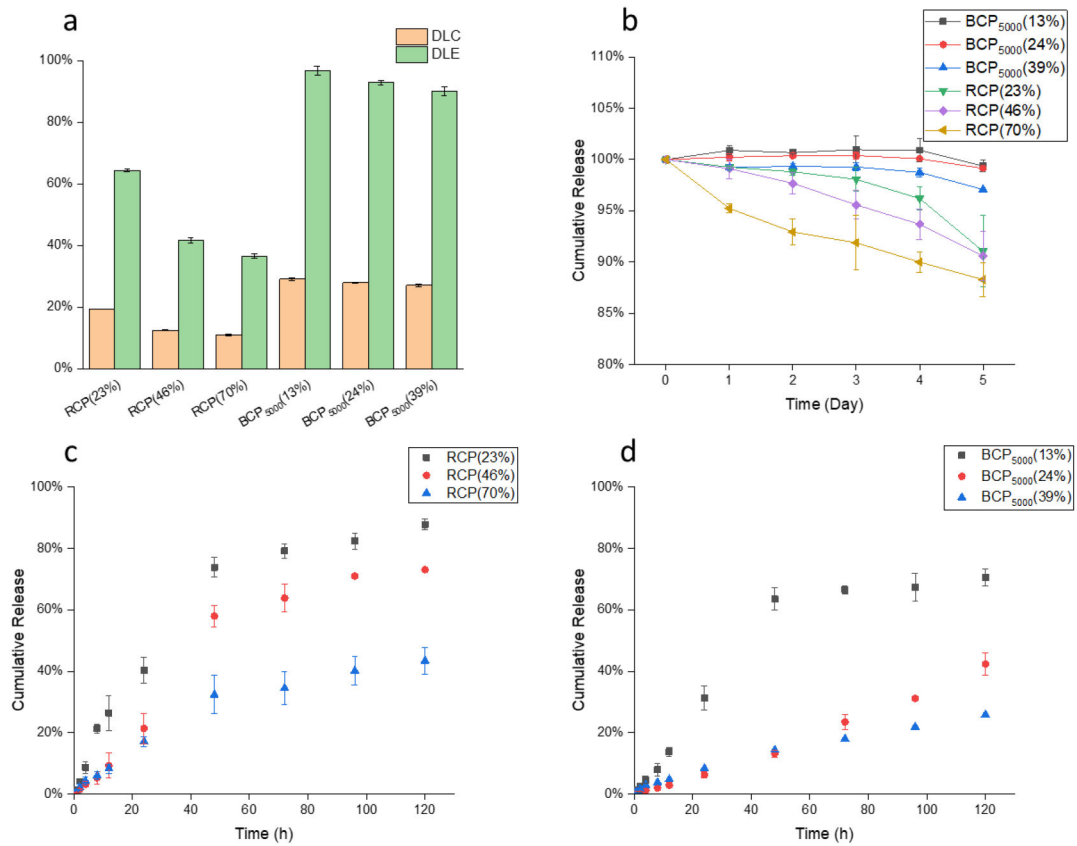
Figure 3.
(a) Drug loading capacity and drug loading efficiency of BCP_{5000} and RCP nanogels with three different crosslinking density; (b) Stability study of BCP_{5000} and RCP nanogels at 10 μM GSH; (c) Release kinetics of RCP at 10 mM GSH; (d) Release kinetics of BCP_{5000} at 10 mM GSH.
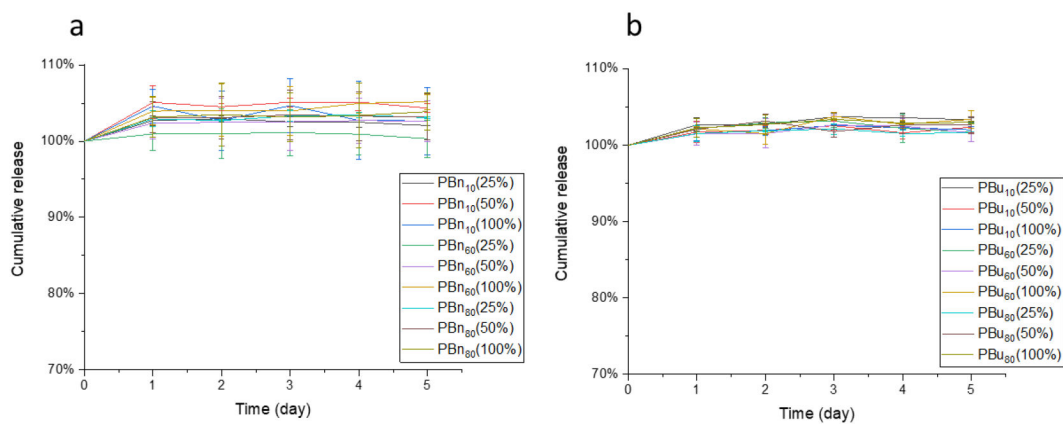
Figure 4.
(a) Encapsulation stability of PBn nanogels at 10 μM GSH; (b) Encapsulation stability of PBu nanogels at 10 μM GSH.

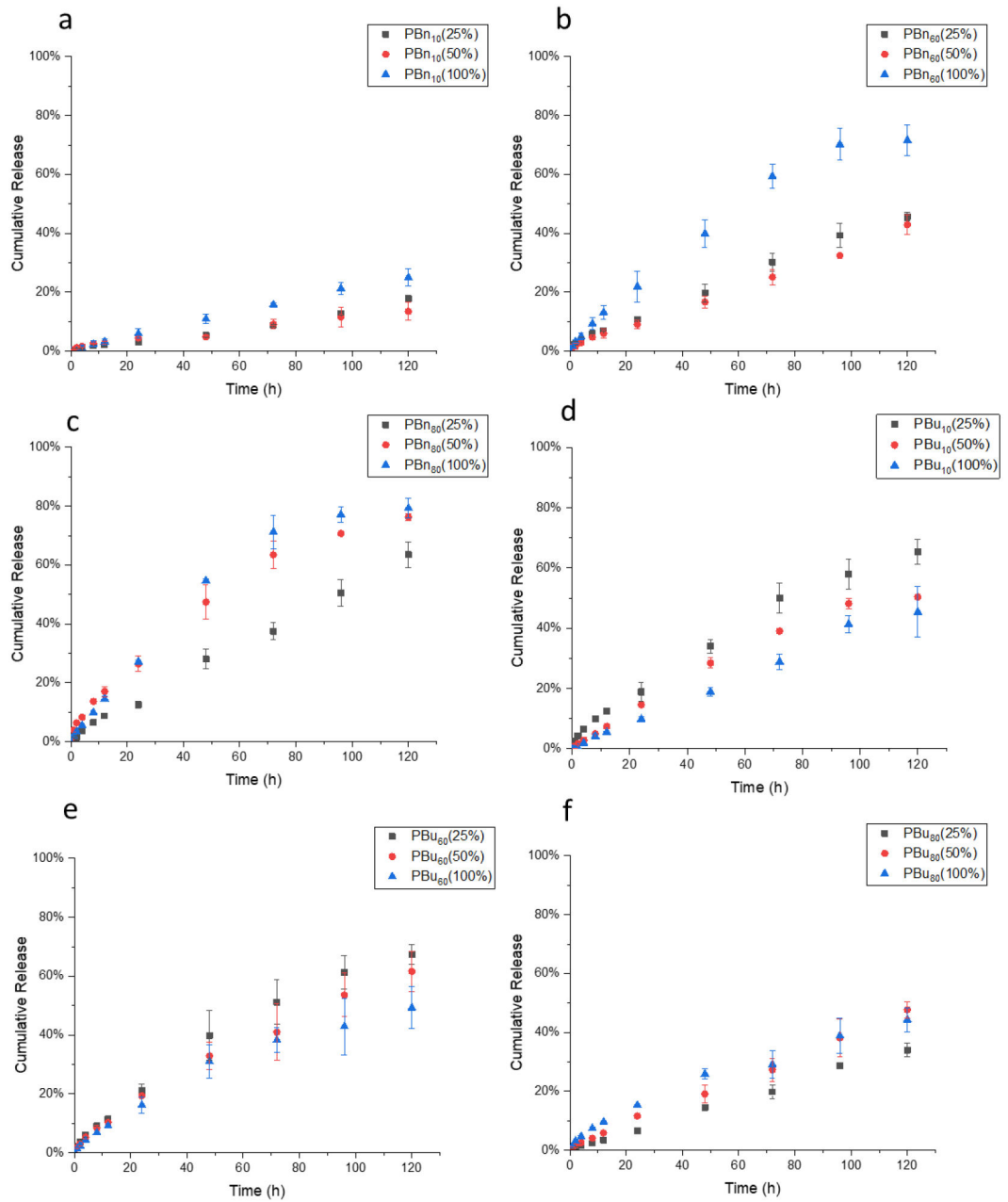**Figure 5.**
(a), (b), (c), Crosslinking dependent release kinetics of PBn_{10}, PBn_{60}, and PBn_{80} nanogels; (d), (e), (f), Crosslinking dependent release kinetics of PBu_{10}, PBu_{60}, and PBu_{80} nanogels.
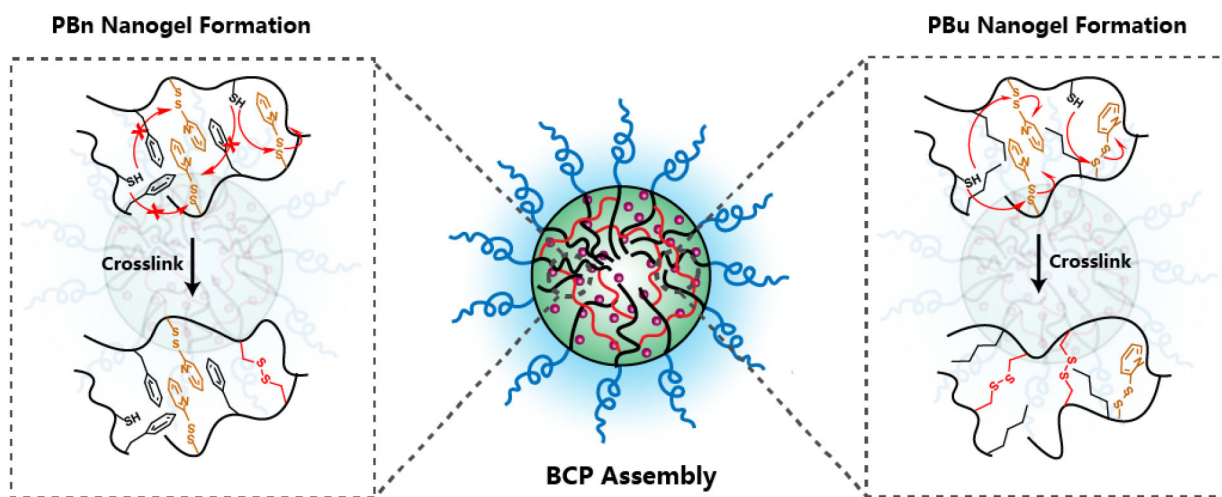
Figure 6.
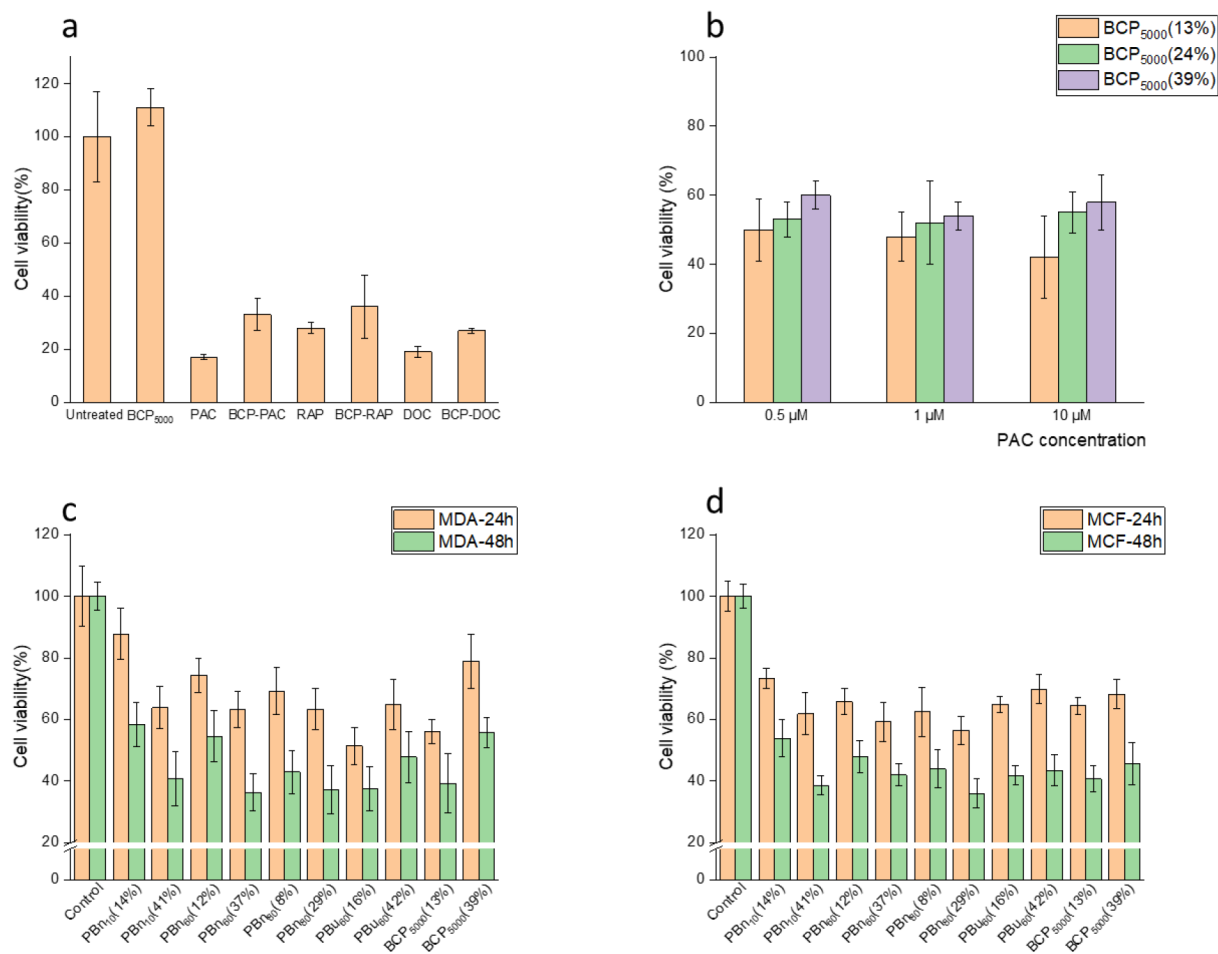Schematic illustration of crosslinking process for PBns and PBus

Figure 7.
(a) Cytotoxicity study of paclitaxel, rapamycin, and docetaxel free drug and the drug encapsulated BCP_{5000} nanogels at 0.5 μM drug concentration in DU-145 cell line. (b) Cytotoxicity study of paclitaxel encapsulated BCP_{5000} nanogel with varied crosslinking density at 0.5, 1, and 10 μM drug concentration in DU-145 cell line. (c), (d) Cytotoxicity study of structrural variant DNC in MDA-MB-231 and MCF-7 cell lines (CPT concentration 0.25 μg/mL, polymer concetration 0.625 μg/mL).

Table 1.

Characterization of the random copolymer(RCP) and block copolymer(BCP)

Polymer	PEG	PDS	$M_n(g \cdot mol^{-1})$	c
BCP_1000	~22 [b]	10	3.5K	1.22
BCP_5000	~113 [b]	10	7.2K	1.25
BCP_10000	~227 [b]	10	12.2K	1.20
RCP	31n [a]	69n [a]	12.4K	1.27

[a] Ratio between PEG monomer and PDS monomer was calculated from ^{1}H NMR results.

[b] Repeat units of PEG for BCPs are calculated based on the average Mn of the PEG chain.

[c] Results are generated by GPC (DMF) using poly(ethylene glycol) as standard.

Table 2.

Structural variants in block copolymers

Polymer	PEG 5000[a]	PDS[a]	Bn[a]	Bu[a]	Mn(g.mol-1)[b]	
PBn$_{10}$	1	9	1	-	7.1K	1.24
PBn$_{60}$	1	4	6	-	7.0K	1.32
PBn$_{80}$	1	2	8	-	7.1K	1.25
PBu$_{10}$	1	9	-	1	6.8K	1.20
PBu$_{60}$	1	4	-	6	6.8K	1.28
PBu$_{80}$	1	2	-	8	6.7K	1.24

[a]Ratio between PEG 5000 RAFT, PDS monomer, and benzyl or butyl monomer are calculated from ^{1}H NMR results.

[b]Results are generated by GPC(DMF) using poly(ethyleneglyco) as standard.

Table 3.

DLC of PBn_{60} and PBu_{60} for camptothecin, paclitaxel, and rapamycin

Drug	LogP[a]	DLC-PBn$_{60}$(%)	DLC-PBu$_{60}$(%)
Camptothecin	1.74	29.4±0.8[b]	29.3±0.2
Docetaxel	2.4	26.5±0.2[c]	26.1±0.3
Paclitaxel	3	27.3±0.4[c]	26.3±0.4
Rapamycin	4.3	28.8±0.7[c]	28.3±0.5

[a] LogP values are collected from the DrugBank website.

[b] Results are generated by the UV-vis method.

[c] Results are generated by HPLC using a UV detector.